



# Preparation and Characterization of Anionic Composite Hydrogel for Dyes Adsorption and Filtration: Non-linear Isotherm and Kinetics Modeling

Adel Mokhtar<sup>1,2</sup> · Soumia Abdelkrim<sup>1</sup> · Amina Sardi<sup>3</sup> · Amina Benyoub<sup>2</sup> · Hadj Besnaci<sup>2</sup> · Rachida Cherrak<sup>4</sup> · Mohammed Hadjel<sup>4</sup> · Bouhadjar Boukoussa<sup>1,5</sup>

Published online: 31 March 2020

© Springer Science+Business Media, LLC, part of Springer Nature 2020

## Abstract

An anionic, low-cost, and environmentally friendly composite PVA/Agar/Bentonite (PAB) hydrogel was prepared via self-assembly method, then evaluated as an adsorbent for both cationic methylene blue (MB) and anionic Congo red (CR) dyes using static (batch adsorption) and dynamic (column filtration) procedures. The structural/textural and morphological features of the hydrogel were investigated by X-ray diffraction, thermogravimetric analysis, Fourier transform infrared spectroscopy, zeta potential measurements and scanning electronic microscopy. The nonlinear forms of first-order and second-order kinetic model, and nonlinear forms of Langmuir–Freundlich, Redlich–Peterson, Langmuir and Freundlich isotherm model were used to study the equilibrium adsorption. The adsorption kinetics of MB and CR dyes onto composite hydrogel followed the nonlinear form of pseudo-second-order model with the adsorption capacity of 107.45 and 42.05 mg/g, respectively. The equilibrium data were fitted well to the nonlinear Langmuir–Freundlich model for MB dye and nonlinear form of Langmuir model for CR dye, which were confirmed by  $R^2$ , MSE and EABS values. Using the column purification method, the composite hydrogel PAB promotes the removal of the MB and CR pollutants by maintaining the concentrations of the filtrate solutions below 0.1 mg/L, even when the volume of the dye reaches 20 mL.

**Keywords** Agar · Hydrogel · Bentonite · Adsorption · Column · Composite · Dye

**Electronic supplementary material** The online version of this article (<https://doi.org/10.1007/s10924-020-01719-6>) contains supplementary material, which is available to authorized users.

✉ Adel Mokhtar  
mokhtar.adel80@gmail.com; adel.mokhtar@cu-relizane.dz

<sup>1</sup> Laboratoire de Chimie des Matériaux LCM, Université Oran1 Ahmed Ben Bella, El- Mnaouer, BP 1524, 31000 Oran, Algeria

<sup>2</sup> Département de Génie des Procédés, Institut des Sciences et Technologies, Centre Universitaire Ahmed Zabana, Relizane, Algeria

<sup>3</sup> Département de Chimie, Faculté des Sciences Exactes et Informatique, Université Hassiba Ben Bouali, 02000 Chlef, Algeria

<sup>4</sup> Laboratoire des Sciences, Technologie et Génie des Procédés (LSTGP), Université des Sciences et Technologie d'Oran Mohamed Boudiaf USTOMB, El-Menouar, BP 1505, 31000 Oran, Algeria

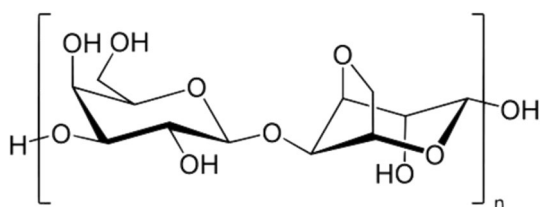
<sup>5</sup> Département de Génie des Matériaux, Faculté de Chimie, Université des Sciences et de la Technologie Mohamed Boudiaf, El-Mnaouer, BP 1505, 31000 Oran, Algeria

## Introduction

The pulse increment, regurgitating, stun, cyanosis, jaundice, quadriplegia, and tissue defects in people are caused by the overuse of dyes [1–4]. To minimize the effects of these dyes from aquatic ecosystems, the researchers required to combine organic–inorganic materials to obtain interesting elimination properties [5–9]. Moreover, the elaboration of materials to create composites able to eliminate these hazardous dyes was the objective of the scientific community. For this, the preparation of composite beads and chitosan-g-poly (acrylic acid)/vermiculite hydrogel composites were used effectively in the elimination of methylene blue from aqueous solutions [10, 11]. This cationic dye was used in several fields such as paper, hair, cotton; and strainers for medicinal surgery [12, 13], and also known by its dangerous effects such as nausea, dizziness, cyanosis, jaundice and tissue necrosis in humans [14]. Regarding the anionic azo dyes, known by their metabolism, carcinogens, mutagens and their potential danger of bioaccumulation and their exposure

causes allergy problems [15]. For these effects, hydrogels composites were enhanced to remove Congo red anionic dye [16, 17]. As can be seen, the morphological, physical and structural form of adsorbents can play an important role in the adsorption behavior of these hazardous and harmful dyes. Therefore, it is important and necessary to develop an efficient, inexpensive and environmentally friendly material able of treating these dyes.

Bentonite is hydrous aluminium phyllosilicate clay which is a good support of biopolymers. The low cost and eco-friendly are the most important upsides of these solids. The negative charge on its surface due to the isomorphous substitution of  $\text{Si}^{4+}$  in tetrahedral layers by  $\text{Al}^{3+}$  and in octahedral layers by  $\text{Mg}^{2+}$ , giving them a various properties [17, 18]. The specific surface area, high-cation exchange capacity, thermal and chemical stability, provided several structural characteristics, which reinforced them [19, 20], as provided good adsorption [21, 22]. Furthermore, due to their 2:1 arrangement [23], Bentonite can expand and contract the interlayer space while preserving two-dimensional



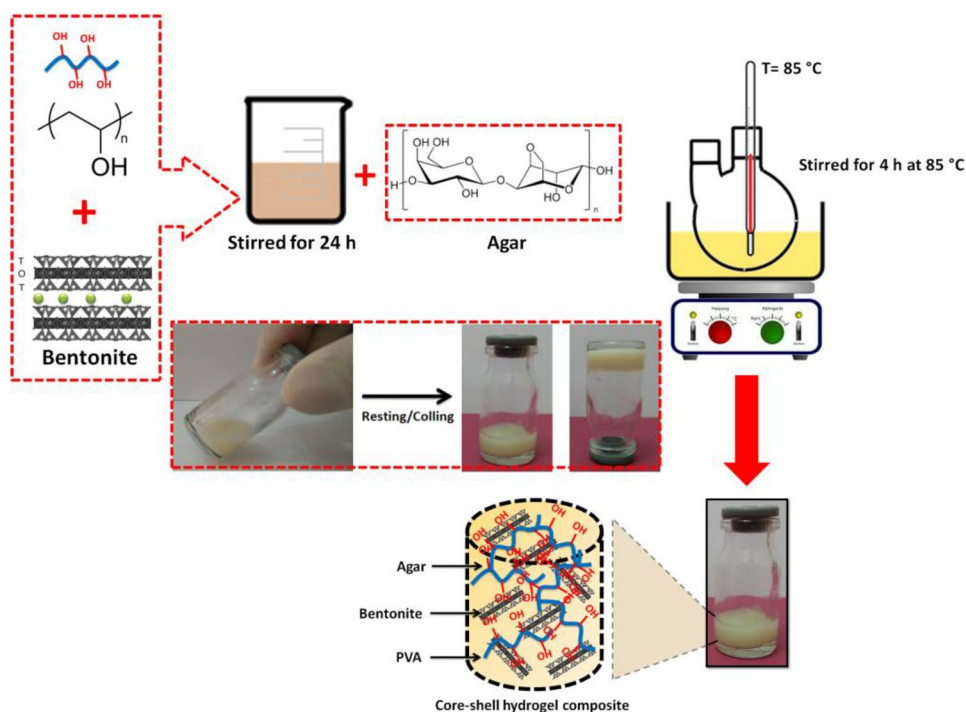
**Scheme 1** Agar structure

crystallographic integrity. A few researchers have used these solids alone for filtration and dye removal, given that Zhao et al. used Halloysite as an effective adsorbent nano-material for the removal of both types of cationic and anionic dyes and also as a water filtration system [24]. Researchers multiply efforts to combine these functional characteristics with inorganic or organic substances to preserve our environment [25, 26].

Agar is a low-cost biodegradable and nontoxic poly-anionic biopolymers with a large number of oxygen-containing functional groups (see Scheme 1), these favorable abundant groups can react via a dehydration reaction and/or the formation of hydrogen bonding. In addition to this, it can be enhanced the composite hydrogel by stabilizing the sheets of clay minerals used. For these describe properties, to build the 3D microstructure the agar was chosen to enhance the stabilization of the bentonite sheets and to remove a large amounts of polluted water in aqueous solutions. Indeed, it is suspected that the abundant oxygen (OH) groups will react by both a hydration reaction and a hydrogen bond for composite hydrogel formation [27–29].

For mentioned reasons, we have prepared composite hydrogel PVA/Agar/Bentonite (PAB) using PVA polymers, layered aluminosilicate material, and agar as precursors (Fig. 1). The clay is expected to offer raised stability and adsorption capacity for water treatment applications. To our cognition, this is the first report using PVA, an Algerian natural clay and agar for the preparation of a composite hydrogel for the removal of cationic and anionic dyes from wastewater. In this line of work, the composite hydrogel PAB

**Fig. 1** Preparation procedure of composite hydrogel PAB, the image inside is the physical transformation of the hydrogel by cooling or heating



was synthesized to evaluate their adsorption and purification properties using static (batch adsorption) and dynamic (column filtration) procedures. The Effects of different hydrogel amounts and different CR and MB dye concentrations were also examined.

## Materials and Methods

### Materials

The selected and treated bentonite obtained by deposits of Maghnia west of Algeria. The structure of bentonite was confirmed by X-ray diffraction (XRD) (see Figure S1 in the supporting information data). Agar bacteriological grade purchased from Biochem. Polyvinyl alcohol (PVA,  $M_w \approx 130,000$ ) was obtained from Aldrich and deionized water was used for all preparations. The characteristics of the two dyes used, the Congo red as anionic and the Methylene blue as cationic dyes were presented in the Table S1 (see the Supporting data section).

### Preparation of PAB Composite Hydrogel

Composite hydrogel (PAB) was prepared using the following procedure which is schematized in (Fig. 1). 1 g of the selected Bentonite having a cation exchange capacity (CEC) of  $\sim 79$  meq/100 g [30, 31], was dispersed in 50 mL of deionized water and stirred overnight, then sonicated at the frequency of 50 kHz for 10 min. 1 g of PVA solution was prepared separately by dissolving in 25 mL of deionized water at 60 °C. After that a 2 wt% of the agar solution was separately prepared at 85 °C. The PVA/Bentonite solution was mixed with the agar solution and stirred at temperature of 85 °C with stirring speed of 500 rpm for 4 h then sonicated for 10 min.

### Characterization Technique

X-ray powder diffraction patterns were recorded in the  $2\theta$  range of  $2^\circ$ – $70^\circ$  at a scan rate  $2^\circ/\text{min}$ , on a Philips diffractometer model PW 1830, with Ni-filtered  $\text{CuK}\alpha$  ( $\lambda = 1.5406 \text{ \AA}$ ) radiation operated at a tube voltage of 40 kV and a tube current of 30 mA. The Fourier Transforms infrared (FTIR) spectra were recorded between 400 and  $4000 \text{ cm}^{-1}$  on a JASCO 4100 spectrometer. To study the morphology of composite hydrogel PAB, the HIROX SH 400 M SEM–EDS BRUKER scanning electron microscope was used. The sample was coated with carbon and attached to sample holders with carbon tape. In order to follow the evaluation of the thermal stability of hydrogel, thermal analysis (TG, dTG and DTA) was performed in air using a Start Pyris DTA-TGA analyzer, the sample was heated

at 1000 °C with heating rate of  $10^\circ\text{C}/\text{min}$ . A specord 200 plus (analytik jena) UV–Vis spectrophotometer was used to measure the absorbance of the pollutants concentration. The surface charges of the prepared materials was also measured by zeta potential using Zeta-sizer (Nano-ZS model, Malvern Instruments, England) at pHs values of 4, 6, 8, 10, and 12.

### Adsorption Isotherms

Firstly, a constant amount of adsorbent (100 mg) was mixed in 100 mL of MB or CR dye solution. The initial concentrations were varied from 10 to 1000 mg/L for the MB dye and from 10 to 750 mg/L for the CR dye at fixed pH of 4.5 and 6.5, respectively. The mixture was stirred at a temperature of  $25 \pm 1^\circ\text{C}$  under stirring speed  $\sim 200$  rpm. All adsorption experiments were repeated twice to ensure the accuracy of the data obtained. The quantities of MB and CR retained were obtained using the following equation:

$$q_e = \frac{(C_0 - C_e) \cdot V}{m}$$

### Kinetic Studies

Series of CR and MB dyes solutions with known concentration were prepared from a stock solution of 1 g/L for each dye. The experiments were realized at the conditions of temperature of  $25^\circ \pm 1^\circ\text{C}$  and without adjusting the pH values of dyes. The values of MB and CR dyes were close to 4.5 and 6.5, respectively. The removal studies were carried out in 100 mL Erlenmeyer flasks using 100 mg of adsorbent with 100 mL of dye solution (100 mg/L) at  $\sim 200$  rpm on a magnetic stirrer. At the end of the adsorption, the supernatants were recovered by the centrifugation and analyzed by spectrophotometer (UV–Vis Specord 210 Analytik Jena). The influence of the contact time, adsorbent dosage (see Fig. 2S in Supplementary information), and concentration, was evaluated. The absorbed amounts of dyes were measured on the basis of the difference in the concentrations of MB and CR dyes in the aqueous solutions before and after adsorption according to the following equation:

$$q_t = \frac{(C_0 - C_t) \cdot V}{m}$$

### Hydrogel Column Application

In this study approximately 0.25–2 g of hydrogel composite was placed in syringes with defatted cotton at the bottom. The initial concentration used for each dye varies between 20 and 100 mg/L, in which were added at the top of the columns and this for each syringe which contains a defined

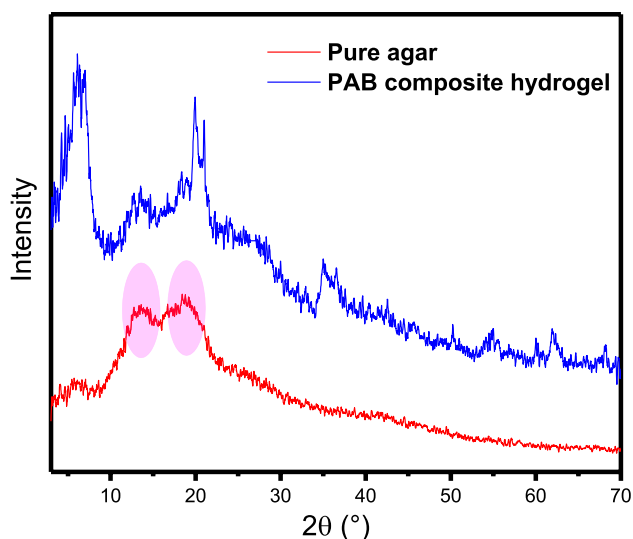


**Fig. 2** Powder XRD patterns of pure Agar and composite hydrogel PAB

mass of composite hydrogel. In total, ten syringes were used containing different masses of composite hydrogel and the concentrations of dye from 20 to 100 mg/L. The clear outlet solution from the bottom of the column was observed with a drop rate of one drop every  $\sim 25$  s under atmospheric pressure with the phenomenon of gravity at the temperature of  $25 \pm 1$  °C. The evaluation of the concentration of the outlet solutions was followed by a UV–Vis spectrophotometer. To study the effect of the dye concentration, the same steps described above for the preparation of the columns were carried out but by varying the concentration of the dyes in the range of 100 to 300 mg/L and fixing the mass of hydrogel composite PAB at 200 mg.

### Kinetic and Isotherm Models

Equilibrium isotherms and adsorption properties describe the adsorbate–adsorbent interactions system and supply complete information about the type of the interaction. For this work, non-linear forms of four different adsorption isotherms notably Langmuir–Freundlich, Redlich–Peterson, Langmuir and Freundlich models were employed to obtain conclusive information on the adsorbent surface characters and its affinity to MB or CR molecules.

Modeling of adsorption isotherm data is important for predicting and comparing adsorption performance. Three-parameter isotherm models are applied in this study available for modeling adsorption data of MB and CR pollutants [7, 32]. The Langmuir–Freundlich (L–F) isotherm is a combination of the Freundlich and Langmuir models used to predict heterogeneous adsorption systems and also to circumvent limitation of the increasing adsorbate concentration

associated with the Freundlich model. At low concentrations of adsorbate it is reduced to Freundlich isotherm; while for a high concentration a monolayer adsorption capacity characteristic of the Langmuir isotherm. The Redlich–Peterson (R–P) isotherm is a combination isotherm featuring the Langmuir and Freundlich isotherms. It is used to represent adsorption equilibrium over a wide range of adsorbate concentration. Its versatility allowed its use either in homogeneous and heterogeneous systems.

To better understand the adsorption behavior, two nonlinear kinetic models are used to test the experimental data. The pseudo-first-order (PFO) and pseudo-second-order (PSO) models were used to evaluate the adsorption of MB and CR dyes on composite hydrogel PAB. Pseudo-first-order and pseudo-second-order Lagergren models are given in Table 1. Where  $q_t$  (mg/g) is the amount of adsorbed dye on the adsorbent at time  $t$  (min),  $q_e$  (mg/g) is the equilibrium adsorption of the pseudo-first-order or pseudo-second-order adsorption,  $k_1$  ( $\text{min}^{-1}$ ) is the pseudo-first-order rate constant, and  $k_2$  (g/mg min) is the pseudo-second-order rate constant.

### Error Functions Application

Error functions are statistics that quantify the error between the model parameters and the experimental values and else by to evaluate the validity and define the optimal fit relation of these models. The mean squared error (MSE) is calculated by the following equation [37, 38]:

$$MSE = \frac{1}{n} \sum_{i=1}^n (q_{cal} - q_{exp})^2$$

The sum of absolute error (EABS) is calculated using the following equation:

$$EABS = \sum_{i=1}^n |q_{exp} - q_{cal}|$$

where  $q_{cal}$  and  $q_{exp}$  refer to the calculated and experimental data and  $n$  is the total number of data points.

## Results and Discussion

### Characterizations of Composite Hydrogel PAB

#### XRD Analysis

XRD patterns of the bentonite, pure agar and PAB composite hydrogel, measured between  $2^\circ$  and  $70^\circ$ , are shown in Fig. 2. The X-ray diffraction (XRD) pattern of bentonite exhibited reflection (001) corresponding to the basal spacing,  $d_{001}$ , of 12.60 Å characteristics of the sodic form (see Fig. 1S in the

**Table 1** The Kinetics and isotherms models with their nonlinear forms

Models	Nonlinear equations	Plot	Parameters	References
PFO	$q_t = q_e(1 - e^{-k_1 t})$	$q_t$ Vs. $t$	$q_e$ is the adsorbed amount at equilibrium, (mg/g), $q_t$ is the adsorb amount per unit weight of adsorbent at time (mg/g), $k_1$ is the rate constant of PFO sorption ( $\text{min}^{-1}$ )	[33, 34]
PSO	$q_t = \frac{k_2 q_e^2 t}{1 + k_2 q_e t}$		$q_t$ and $q_e$ have the same meaning as in the PSO model and $k_2$ is the rate constant of PSO model (g/mg min)	
L-F	$q_e = \frac{k_{LF} C_e^\beta}{1 + a_{LF} C_e^\beta}$	$q_e$ Vs. $C_e$	$q_e$ is the adsorbed amount at equilibrium, (mg/g), $C_e$ is the concentration of adsorbate in the solution at equilibrium (mg/L). $k_{LF}$ (L/g), $a_{LF}$ (L/mg) $^\beta$ and $\beta$ (dimensionless) are L-F isotherm constants	[35, 36]
R-P	$q_e = \frac{k_{RP} C_e}{1 + a_{RP} C_e^\beta}$		$q_e$ is the adsorbed amount at equilibrium, (mg/g), $C_e$ is the concentration of adsorbate in the solution at equilibrium (mg/L). $k_{RP}$ (L/g), $a_{RP}$ (L/mg) $^\beta$ and $\beta$ (dimensionless) are R-P isotherm constants	
L	$q_e = \frac{q_{max} b_L C_e}{1 + b_L C_e}$	$q_e$ Vs. $C_e$	$q_e$ is the adsorbed amount of dye per unit mass of adsorbent (mg/g). $b$ is the Langmuir constant related to the adsorption capacity (L/g). $C_e$ is the concentration of adsorbate in the solution at equilibrium (mg/L). $q_{max}$ is the maximum uptake per unit mass (mg/g)	[37]
F	$q_e = k_f C_e^{1/n}$		$C_e$ has the same meaning as in the Langmuir isotherm. $k_f$ is the Freundlich constant. $n$ is the empirical parameter representing the energetic heterogeneity of the adsorption sites (dimensionless)	

Supplementary data) [39]. The X-ray diffraction pattern of PVA/bentonite sample show that the bentonite was intercalated with PVA. The basal spacing  $d_{001}$  of bentonite expands from 12.60 to 14.29 Å. This increase is thought to occur by absorption of PVA over the surface of the clay sheets (see Fig. 2S in the Supplementary data). The X-ray diffraction pattern of pure agar showed the presence of two-diffraction peaks at  $2\theta$  values of  $12.90^\circ$  and  $19.04^\circ$  characteristic to the hydrated crystalline structure and to the existence of an amorphous structure, respectively [28]. The XRD pattern of composite hydrogel PAB showed that the clay peaks position does not change but their intensity was reduced, suggesting that during the reaction with PVA polymer is not completely intercalated between the interlayer space of bentonite, probably the majority of polymer was adsorbed only at the clay surface which provides a basal spacing of  $d_{001} = 15.21$  Å (see the Supplementary data). The two characteristics peaks of pure agar are observed in the composite hydrogel, which signify their crushing by agar during physical cross-linking process, it may be related to their composition with the biopolymer because agar has an amorphous nature which can probably affect hydrogel crystallinity. To sum up, the composite hydrogel raised a decrease in crystallinity probably attributed to the presence of a high number of hydrogen bonds in the agar matrix.

### FTIR Analysis

The characteristics functional groups of pure agar, PVA, bentonite, and prepared PVA hydrogel sample were characterized by FT-IR spectrum (Fig. 3). The FTIR spectrum of pure agar contains a broad band at  $3323 \text{ cm}^{-1}$  related to

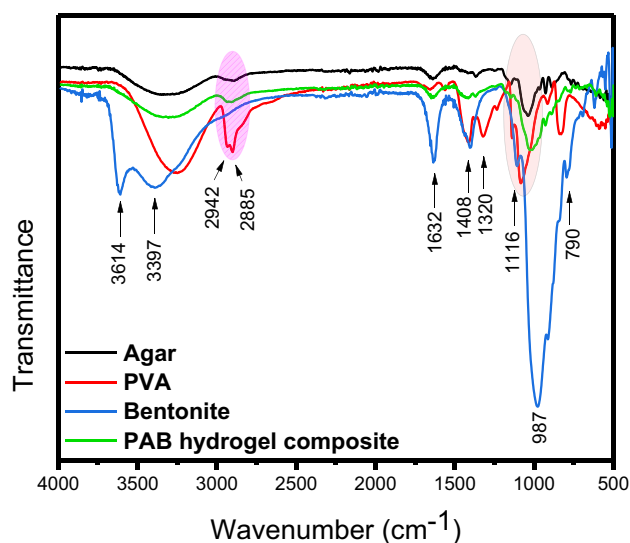


**Fig. 3** FTIR spectra of pure Agar, PVA, Bentonite and composite hydrogel PAB

the stretching vibration of  $-\text{OH}$ , also indicating that agar contains large amounts of hydroxyl groups. The adsorption bands located at 2929, 1656, and  $1367 \text{ cm}^{-1}$  correspond to the C–H stretching vibration of  $-\text{CH}_3$  and  $-\text{CH}_2$  groups, and the stretching vibration of the formation bonds of (N–H) and (C=O) groups, respectively [40, 41]. The vibration bands of bentonite are described as follows: the OH stretching band observed in the region of  $3631\text{--}3444 \text{ cm}^{-1}$ , the Si–O–Si stretching bands located at  $1091\text{--}1039 \text{ cm}^{-1}$ , and the Si–O stretching vibration band located at  $795 \text{ cm}^{-1}$  [39, 42–44]. The FTIR spectrum of PVA polymer revealed

a broad peak around  $3425\text{ cm}^{-1}$  indicating stretching of hydroxyl groups and bands at  $2942\text{ cm}^{-1}$  and  $2885\text{ cm}^{-1}$  due to C–H stretching, similar as was presented in previous works [45].

The infrared spectrum of PAB hydrogel shows the presence of numerous vibration bands characteristic of agar, PVA, and bentonite as well as new absorption bands appeared. The disappearance of band at  $3614\text{ cm}^{-1}$  belonging to the Si–OH groups in clay as well as the decreasing relatively in the transmittance of OH stretching vibration band located at  $3320\text{ cm}^{-1}$  compared to original materials probably due to the formation of hydrogen bonding between clay and polymers [10–12]. Additionally, the presence of elongation vibration bands in the Si–O–Si bond at  $1116\text{ cm}^{-1}$  is characteristic to the bentonite [13, 14], the bands at  $3942\text{ cm}^{-1}$  and  $2885\text{ cm}^{-1}$  belonged to the stretching vibration peaks of  $\text{CH}_3$  and  $\text{CH}_2$  [15], respectively. To sum, the PVA, bentonite, and agar were successfully compounded to form the composite hydrogel through physical cross-linking process with the dominant interaction through hydrogen bonds forces.

## SEM Analysis

Scanning electron microscopy is probably the most distributed analytical technique to characterize the physical properties such as morphology, shape, size or size distribution of materials at the microscale. As shown in Fig. 4, it was observed that the surface morphology of the hydrogel reveals no phase separation between the materials used, i.e. polymer and bentonite in the composite hydrogel, suggesting that the bentonite had been successfully immobilized on agar matrix. In addition, the morphology of the composite hydrogel surface is compact and less smooth [46, 47]. The surface of the composite is uniform, embedded in the matrix with some aggregation of clay, the clay particles are relatively well dispersed in the biopolymer. As summary, this result can be attributed to the fact that the long chains of the polymer could reduce the interaction between the hydrophilic (–OH) groups and improve the compatibility of the clay with the agar matrix.

## Thermal Analysis

Thermo-stability of the PAB hydrogel was evaluated by (TG, dTG and DTA) analysis, the thermal-gravimetric curves are shown in Fig. 5. As can be seen, the first

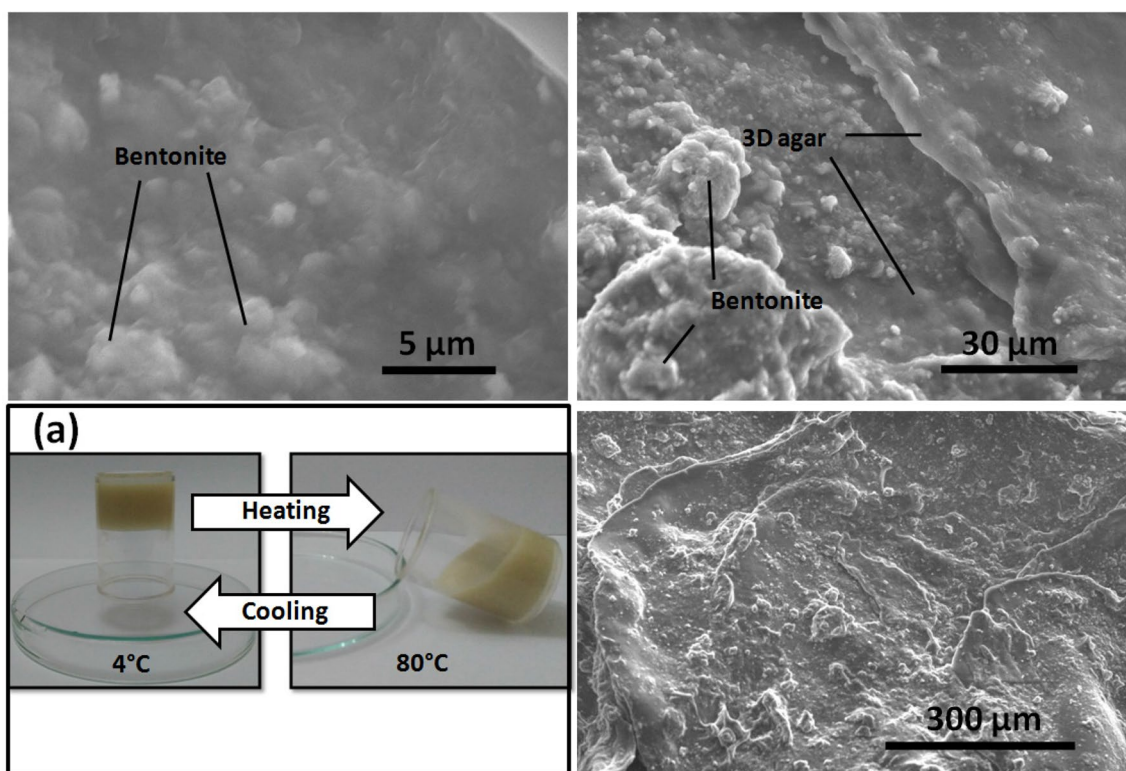
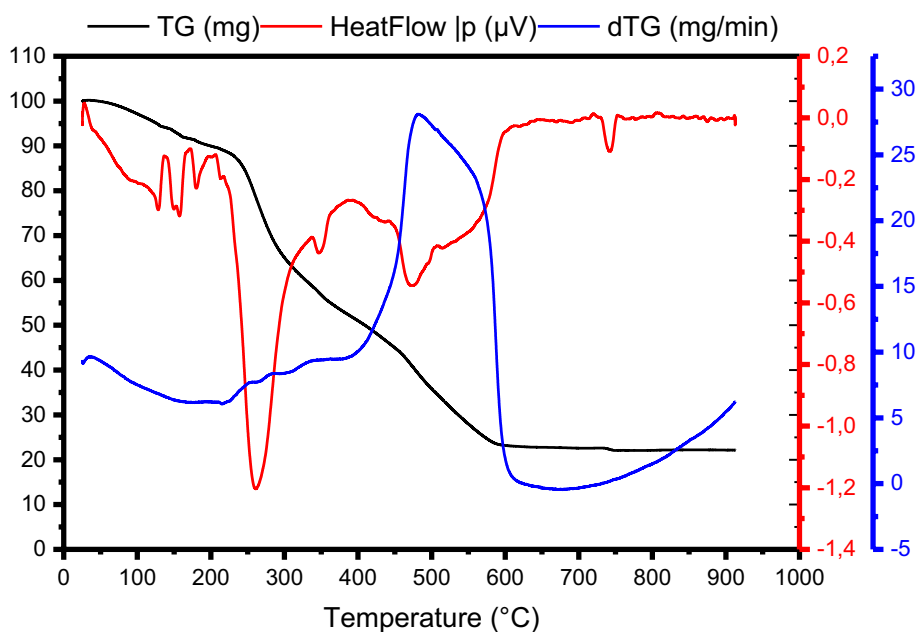


**Fig. 4** Scanning electron micrographs of PAB composite hydrogel; (a) showing transition of PAB hydrogel upon heating and cooling

**Fig. 5** Thermograms (TG, dTG and DTA) of PAB composite hydrogel sample



degradation stage occurs prior 210 °C with a weight loss of about 10.22% for hydrogel sample which is probably attributed to the evaporation of free and bound water. In addition, the possibility for the polymer to melt at this temperature can probably be another reason for this first degradation step. The second degradation stage localized between 210 and 590 °C with a weight loss 66.56% attributed to the organic part of composite hydrogel that could belong to polymers evaporated, as well as dehydroxylation and decarboxylation of organic reagents. The last degradation with a weight loss of about 1.14% is due to the residues containing bentonite as referred by various authors [48]. As shown, the PAB hydrogel has revealed higher thermal stability [49, 50], probably due to the interactions and physical crosslinking, these interactions which were created between inorganic–organic substances.

### Zeta Potential Measurement

In order to determine the charge and to understand the influence of pH on the hydrogel surface exhibited in Fig. 6, the zero point charge of the prepared hydrogel composite was determined by measuring the zeta potential at different pH values. As expected, the zeta potential of the composite sample is always negative when the pH increases from 4 to 12. This result shows the role of the OH groups present in the hydrogel surface which increases the negativity of the surface, either by the silanol groups of the clay (Si–OH) or by the hydroxyl groups of the polymers [51, 52].

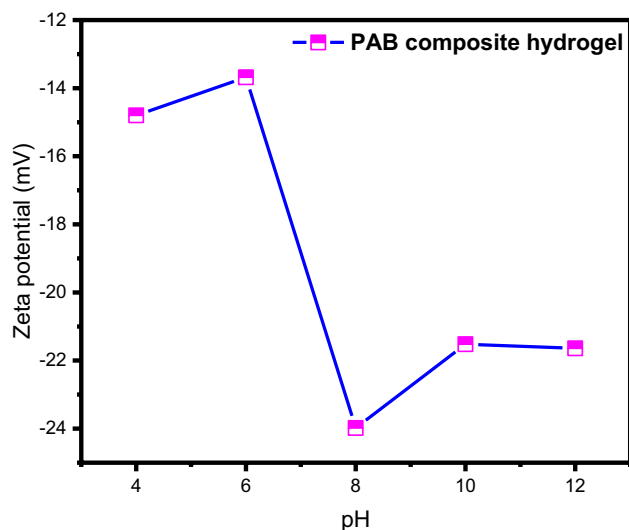


**Fig. 6** Zeta potential curves of composite hydrogel PAB

### Adsorption Study

#### Adsorption Kinetics

The kinetics adsorption of MB and CR dyes onto composite hydrogel PAB was evaluated and the results were given in Fig. 7. The results show a rapid adsorption of MB and CR dyes on the composite hydrogel PAB, suggesting a strong affinity between the dye molecules and the surface of the hydrogel. The time of adsorption equilibrium of MB and

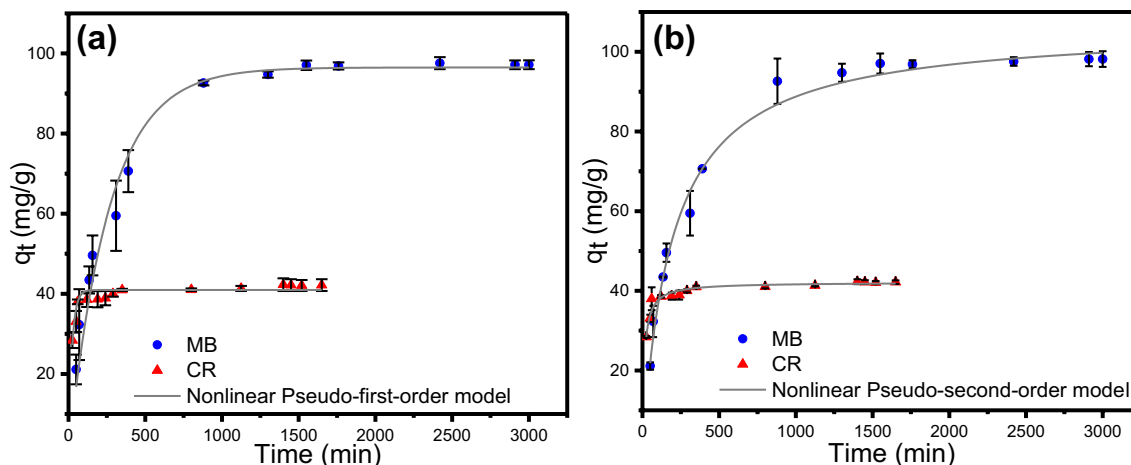


**Fig. 7** Nonlinear adsorption forms of Pseudo-first-order and Pseudo-second-order models for MB and CR dyes onto composite hydrogel PAB (conditions: C = 100 ppm, V = 100 mL; mass of composite = 100 mg; T = 25 ± 1 °C; pH<sub>MB</sub> 4.5 and pH<sub>CR</sub> 6.5)

**Table 2** Pseudo-first-order and pseudo-second-order model parameters and correlation coefficients for MB and CR adsorption onto composite hydrogel PAB

Dyes	Adsorbent	PFO					PSO				
		q <sub>e,cal</sub> mg/g	k <sub>1</sub> min <sup>-1</sup>	R <sup>2</sup>	MSE	EABS	q <sub>e,cal</sub> mg/g	k <sub>2</sub> g/mg min	R <sup>2</sup>	MSE	EABS
MB	PAB	96.071	0.004	0.975	1.056	3.706	107.153	0.0056	0.989	0.065	0.917
CR	PAB	40.696	0.042	0.832	0.271	1.947	42.050	0.088	0.937	0.003	0.214

CR dyes is 2 and 1 day, respectively. It is clearly observed that the MB dye was rapidly adsorbed on the agar surface due to the electrostatic forces and also in the clay galleries. While, for the case of CR molecules, the adsorbent sites are saturated quickly due to the hydrogen bond. The pseudo-first and pseudo-second order models were employed to correlate the kinetics points. As can be seen in Table 2, the regression coefficient R<sup>2</sup> of pseudo-second-order model properly depicts the adsorption process of the MB and CR dyes. The calculated adsorption capacities of MB and CR were determined using the nonlinear pseudo-second-order equation which is found to be 107.15 and 42.05 mg/g, respectively. In addition, the calculation of MSE and ABSE values using the error functions was reinforce this opinion.

**Adsorption Isotherms**

The adsorption isotherms of MB and CR dyes onto composite hydrogel PAB are given in Fig. 8. The adsorbed amount of both dyes increased slowly with increasing the initial concentration leading to an adsorption isotherm type H which is characteristic of monolayer adsorption due to the strong adsorbate–adsorbate interaction. In addition, the experimental data were analyzed by fitting them to the nonlinear forms of Langmuir–Freundlich, Redlich–Peterson, Langmuir and

Freundlich models (see Table 1). According to the isotherms parameters as presented in Table 3, the removal of MB dye using the composite hydrogel PAB was governed by the nonlinear Langmuir–Freundlich model, which is correlates with the calculated of R<sup>2</sup>, MSE and EABS values. For CR dye, the adsorption behavior was fitted well by the nonlinear form of Langmuir isotherm model, with the high coefficient of determination and the less errors values.

**Hydrogel Column Study**

**The Filtration Study of CR and MB Dyes Using Composite Hydrogel PAB Column**

The effect of adsorbent amount and initial dyes concentration using columns process were evaluated. Figures 9 and 10 show the filtration columns and the absorption spectra of the outlet solutions, respectively. As can be seen, in most of the columns, the color of the output solutions was completely disappeared. Except in the case of anionic CR dye at adsorbent masse of 0.25 and 0.5 g of composite PAB, the filtrate was light red corresponds of the concentrations of 6 mg/L and 8 mg/L, respectively. The effect of initial concentrations of the CR



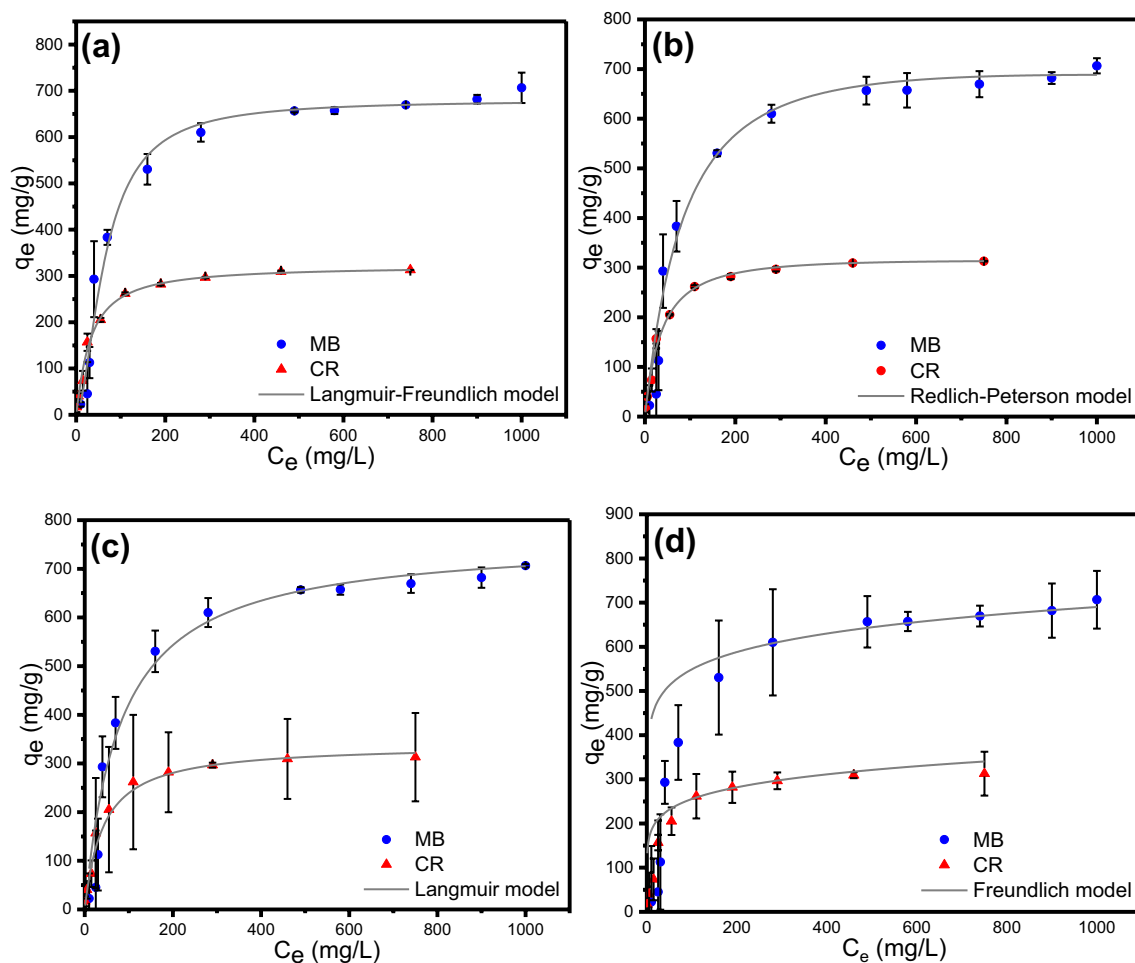


**Fig. 8** Non-linear forms of Langmuir–Freundlich (a), Redlich–Peterson (b), Langmuir (c) and Freundlich (d) models for MB and CR dyes adsorption onto composite hydrogel PAB

and MB dyes were varied in the range of 100–300 mg/L using 20 mL of each dye solution and 200 mg of composite hydrogel PAB. The results showed that the filtrate concentration of MB and CR dyes is kept below 0.1 mg/L even when the dyes solutions volume reaches at 20 mL. It means that the PAB composite hydrogel column can successfully remove CR and MB dyes from the wastewater.

The enlargement of the filtration columns images and the absorption spectra are presented in Fig. 11. The objective was to see well the drops after filtration for each dye. It is clear from the bottom of the column that the color of the outgoing drop visually gives the difference in color before and after the filtration process. This also confirms the effectiveness of the removal of MB and CR dyes by

the composite hydrogel PAB, using the filtration column method.

### Comparative Study

Moreover, according to the adjustment and the kinetic study, the composite hydrogel PAB exhibited a maximum adsorption capacity ( $q_{\max}$ ) of 107.15 mg/g for the adsorption of MB, which is very important compared to the others adsorbents reported in the literature (Table 4). The high capacity with rapid adsorption kinetics implies that the composite hydrogel adsorbent is highly competitive as an effective adsorbent for cationic dyes applications.

**Table 3** Adsorption isotherms parameters for MB and CR dyes onto composite hydrogel PAB

Models	Dye	Parameters			
Langmuir–Freundlich	Methylene Blue	$k_{LF}$ (L/mg)	0.547		
		$\beta$ (L/mg)	1.715		
		$a_{LF}$	8.06E–4		
		$R^2$	0.979		
		MSE	1.865		
		EABS	4.731		
Redlich–Peterson		$k_{RP}$ (L/g)	6.566		
		$\beta$ (L/mg)	1.166		
		$A_{RP}$	2.7E–3		
		$R^2$	0.966		
		MSE	137.645		
		EABS	40.641		
Langmuir		$R^2$	0.979		
		$q_{max}$	762.440		
		$b_L$	0.0124		
		MSE	221.155		
		EABS	51.574		
		$R^2$	0.630		
Freundlich		$k_f$	347.376		
		$1/n$	0.0994		
		MSE	1335.769		
		EABS	126.606		
		Langmuir–Freundlich	Congo Red	$K_{LF}$ (L/mg)	5.946
				$\beta$ (L/mg)	1.152
$a_{LF}$	18.5E–3				
$R^2$	0.991				
MSE	11.714				
EABS	10.823				
Redlich–Peterson		$k_{RP}$ (L/g)	8.594		
		$\beta$ (L/mg)	1.043		
		$A_{RP}$	19.6E–3		
		$R^2$	0.991		
		MSE	6.778		
		EABS	8.233		
Langmuir		$R^2$	0.998		
		$q_{max}$	339.554		
		$b_L$	0.02381		
		MSE	10.363		
		EABS	10.179		
		$R^2$	0.790		
Freundlich		$k_f$	132.615		
		$1/n$	0.1423		
		MSE	158.123		
		EABS	39.764		

## Adsorption Mechanism

The fixation of anionic and cationic dyes is probably linked to the presence of the various functional groups. The influence the adsorption capacity of these pollutants provided various adsorbate-adsorbent interactions such as Hydrogen bonding [61], electrostatic interaction [62],  $\pi$ - $\pi$  stacking [63], and Van der Waals forces [64]. In the present work, Hydrogen bonding plays a significant role (see Fig. 12). Hence, for both dyes which have mobile hydrogen atoms capable of forming bonds with Si–O and OH groups of composite hydrogel PAB. In the case of the anionic CR dye adsorption, hydrogen bonding force is preponderant. Compared to cationic MB dye and the negative surface charge of composite hydrogel (confirmed previously by zeta potential measurements), to give an increase of adsorption efficiency indicating the influence by electrostatic interaction.

## Conclusions

The composite hydrogel PAB was successfully prepared via self-assembly method, for removal and filtration polluted water. Bentonite participated in the establishment of hydrogel network, leading to their homogeneous dispersion in the agar matrix. The composite hydrogel demonstrated higher adsorption capacity for cationic MB dye. The adsorption kinetics of dyes onto the composite hydrogel followed the nonlinear form of pseudo-second-order model with adsorbed theoretical quantities of 107.15 and 42.05 mg/g for MB and CR dyes, respectively. The equilibrium data were fitted well to the nonlinear form of Langmuir–Freundlich model for MB dye and the nonlinear form of Langmuir model for CR dye, which were confirmed with high  $R^2$  and the less error functions values. The hydrogen bonding plays an important role in this adsorption mechanism, due to the presence of mobile hydrogen atoms in both pollutants which are able to form bonds with the Si–O and OH groups of the hydrogel composite. The mechanism of adsorption of the anionic CR dye is dominated by this force. For the cationic MB dye, the negative surface charge of the composite hydrogel introduces electrostatic interaction forces. The column filtration process was shown promising results for eliminated both cationic and anionic dyes. The morphology of the PAB composite hydrogel promotes the removal of dyes by keeping the filtrate solutions concentration below 0.1 mg/L even when the volume of the dye solutions reaches to 20 mL. This means that the composite hydrogel PAB column can be successfully remove the CR and MB dyes from the wastewater.

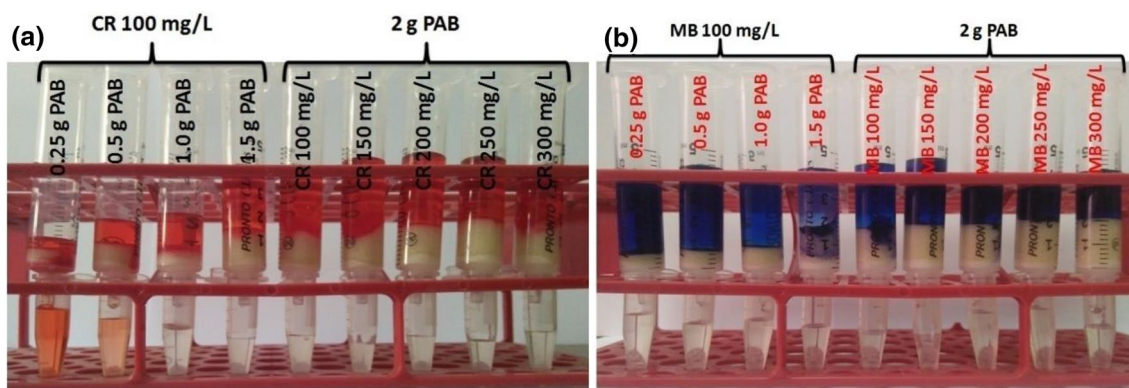


**Fig. 9** Elimination of dyes from water using filtration columns procedure, (a and b) pictures of the apparatus used for filtration MB (a) and CR (b) solutions (Pictures were taken during the study)

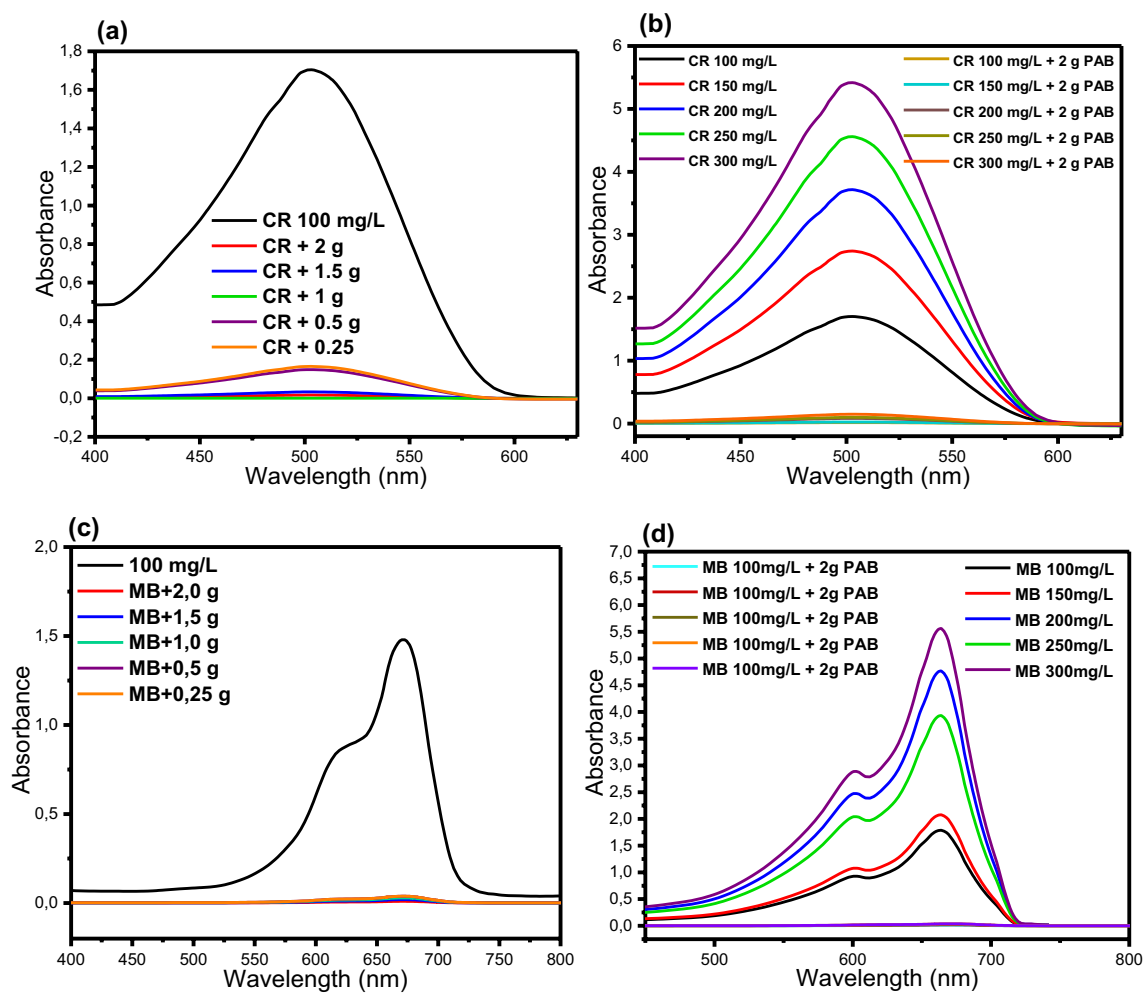


**Fig. 10** UV-Vis absorbance spectra of dyes solutions, (a) at PAB hydrogel amounts (CR, 100 mg/L and 20 mL), (b) at CR dye concentrations (200 mg and 20 mL), (c) at PAB hydrogel amounts (MB dye 100 mg/L and 20 mL), (d) at MB dye concentrations (200 g and 20 mL)

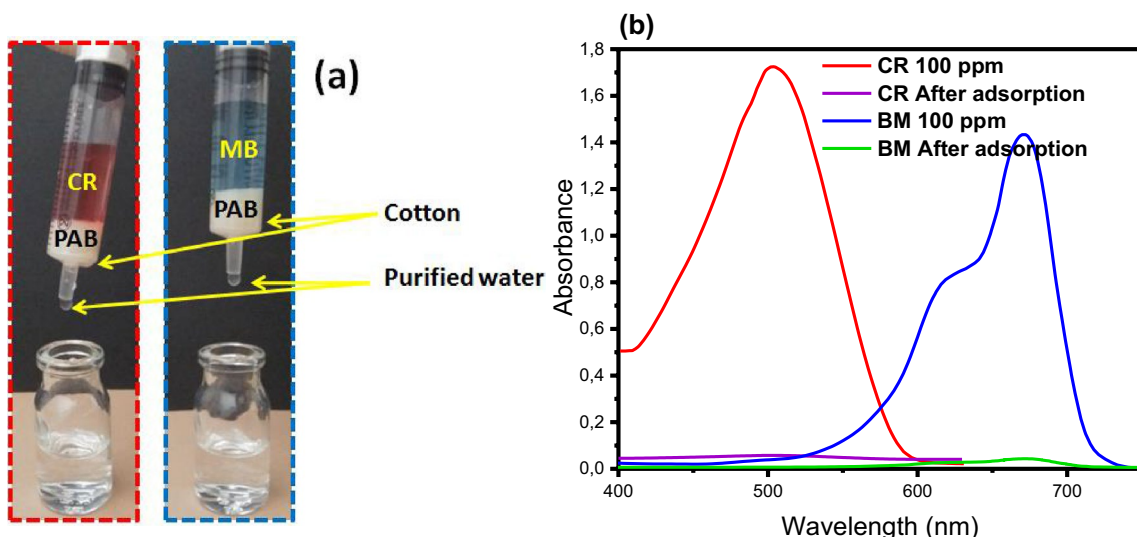


**Fig. 11** Elimination of MB and CR dyes from water by filtration columns process. **a** Images of the apparatus used for filtration and the solution of MB and CR dyes, condition (concentration: 100 mg/L and

masse of hydrogel: 100 mg). **b** Absorption spectrum of MB CR solutions before and after filtration process

**Table 4** Comparison of the maximum adsorption capacity of PAB hydrogel adsorbent with other composite adsorbents reported in the literature

Adsorbent	Adsorbate	q <sub>max</sub> (mg/g)	References
Hydrogel based on waste corn stalk	MB	49.01	[53]
Polyacrylamide/polyacrylate/gum Arabic		48.00	[54]
Gelatin/bentonite composite beads		70.79	[55]
PVA/SBA-15		77.00	[56]
Zeolitic imidazolate framework-67		50.50	[57]
PAB hydrogel composite		107.15	In this work
Alginate-bentonite composite beads	CR	111.07	[58]
Chitosan/montmorillonite		54.50	[59]
Reagent NiO nanoparticles		39.70	[60]
Hierarchical Ni(OH) <sub>2</sub> nanosheets		82.90	[60]
Zeolitic imidazolate framework-67		714.30	[57]
PAB hydrogel composite		42.05	In this work

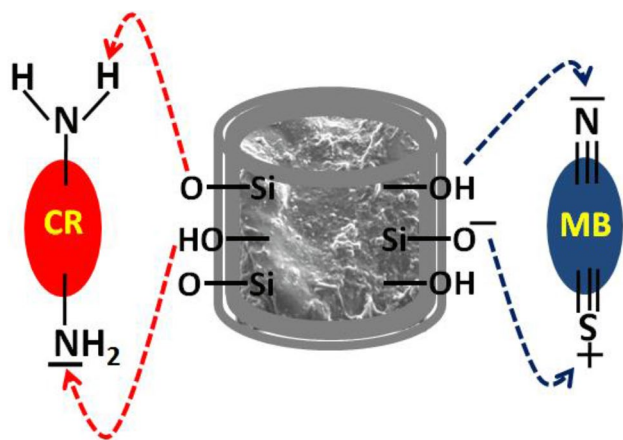


**Fig. 12** Plausible mechanism for interaction of CR and MB dyes with composite hydrogel PAB

**References**

1. Kunz A, Mansilla H, Duran N (2002) A degradation and toxicity study of three textile reactive dyes by ozone. *Environ Technol* 23(8):911–918
2. Li S (2010) Removal of crystal violet from aqueous solution by sorption into semi-interpenetrated networks hydrogels constituted of poly (acrylic acid-acrylamide-methacrylate) and amylose. *Biores Technol* 101(7):2197–2202
3. Boukoussa B, Hamacha R, Morsli A, Bengueddach A (2017) Adsorption of yellow dye on calcined or uncalcined Al-MCM-41 mesoporous materials. *Arab J Chem* 10:S2160–S2169
4. Medjdoubi Z, Hachemaoui M, Boukoussa B, Hakiki A, Bengueddach A, Hamacha R (2019) Adsorption behavior of Janus Green B dye on Algerian diatomite. *Mater Res Exp* 6(8):085544
5. Shaban M, Abukhadra MR, Shahien M, Ibrahim SS (2018) Novel bentonite/zeolite-NaP composite efficiently removes methylene blue and Congo red dyes. *Environ Chem Lett* 16(1):275–280

6. Kumari HJ, Krishnamoorthy P, Arumugam T, Radhakrishnan S, Vasudevan D (2017) An efficient removal of crystal violet dye from waste water by adsorption onto TLAC/Chitosan composite: a novel low cost adsorbent. *Int J Biol Macromol* 96:324–333
7. Djelad A, Mokhtar A, Khelifa A, Bengueddach A, Sassi M (2019) Alginate-whey an effective and green adsorbent for crystal violet removal: kinetic, thermodynamic and mechanism studies. *Int J Biol Macromol* 139:944–954
8. Mokhtar A, Abdelkrim S, Djelad A, Sardi A, Boukoussa B, Sassi M, Bengueddach A (2020) Adsorption behavior of cationic and anionic dyes on magadiite-chitosan composite beads. *Carbohydr Polym* 229:115399
9. Boukoussa B, Hakiki A, Moulai S, Chikh K, Kherroub DE, Bouhadjar L, Guedal D, Messaoudi K, Mokhtar F, Hamacha R (2018) Adsorption behaviors of cationic and anionic dyes from aqueous solution on nanocomposite polypyrrole/SBA-15. *J Mater Sci* 53(10):7372–7386
10. Ai L, Li M, Li L (2011) Adsorption of methylene blue from aqueous solution with activated carbon/cobalt ferrite/alginate composite beads: kinetics, isotherms, and thermodynamics. *J Chem Eng Data* 56(8):3475–3483
11. Liu Y, Zheng Y, Wang A (2010) Enhanced adsorption of Methylene Blue from aqueous solution by chitosan-g-poly (acrylic acid)/vermiculite hydrogel composites. *J Environ Sci* 22(4):486–493
12. Levin RL, Degrange MA, Bruno GF, Del Mazo CD, Taborda DJ, Griotti JJ, Bouillon FJ (2004) Methylene blue reduces mortality and morbidity in vasoplegic patients after cardiac surgery. *Ann Thorac Surg* 77(2):496–499
13. Thakur S, Pandey S, Arotiba OA (2016) Development of a sodium alginate-based organic/inorganic superabsorbent composite hydrogel for adsorption of methylene blue. *Carbohydr Polym* 153:34–46
14. Vadivelan V, Kumar KV (2005) Equilibrium, kinetics, mechanism, and process design for the sorption of methylene blue onto rice husk. *J Colloid Interface Sci* 286(1):90–100
15. Ghorai S, Sarkar AK, Panda AB, Pal S (2013) Effective removal of Congo red dye from aqueous solution using modified xanthan gum/silica hybrid nanocomposite as adsorbent. *Biores Technol* 144:485–491
16. Chatterjee S, Lee MW, Woo SH (2010) Adsorption of congo red by chitosan hydrogel beads impregnated with carbon nanotubes. *Biores Technol* 101(6):1800–1806
17. Bhattacharyya R, Ray SK (2015) Removal of congo red and methyl violet from water using nano clay filled composite hydrogels of poly acrylic acid and polyethylene glycol. *Chem Eng J* 260:269–283
18. Mokhtar A, Bennabi F, Abdelkrim S, Sardi A, Boukoussa B, Souana A, Bengueddach A, Sassi M (2020) Evaluation of intercalated layered materials as an antimicrobial and drug delivery system: a comparative study. *J Incl Phenom Macrocycl Chem* 96:353–364
19. Shi L-n, Zhang X, Chen Z-l (2011) Removal of chromium (VI) from wastewater using bentonite-supported nanoscale zero-valent iron. *Water Res* 45(2):886–892
20. Motshekga SC, Ray SS, Onyango MS, Momba MN (2013) Microwave-assisted synthesis, characterization and antibacterial activity of Ag/ZnO nanoparticles supported bentonite clay. *J Hazard Mater* 262:439–446
21. Pandey S, Ramontja J (2016) Natural bentonite clay and its composites for dye removal: current state and future potential. *Am J Chem Appl* 3(2):8
22. Anirudhan T, Ramachandran M (2015) Adsorptive removal of basic dyes from aqueous solutions by surfactant modified bentonite clay (organoclay): kinetic and competitive adsorption isotherm. *Process Saf Environ Prot* 95:215–225
23. Bergaya F, Lagaly G (2013) General introduction: clays, clay minerals, and clay science. *Dev Clay Sci* 1:1–19
24. Zhao Y, Abdullayev E, Vasiliev A, Lvov Y (2013) Halloysite nanotubule clay for efficient water purification. *J Colloid Interface Sci* 406:121–129
25. Tirtom VN, Dinçer A, Becerik S, Aydemir T, Çelik A (2012) Comparative adsorption of Ni(II) and Cd(II) ions on epichlorohydrin crosslinked chitosan–clay composite beads in aqueous solution. *Chem Eng J* 197:379–386
26. Bée A, Obeid L, Mbolantenaina R, Welschbillig M, Talbot D (2017) Magnetic chitosan/clay beads: A magsorbent for the removal of cationic dye from water. *J Magn Magn Mater* 421:59–64
27. Tao Y, Kong D, Zhang C, Lv W, Wang M, Li B, Huang Z-H, Kang F, Yang Q-H (2014) Monolithic carbons with spheroidal and hierarchical pores produced by the linkage of functionalized graphene sheets. *Carbon* 69:169–177
28. Xie T, Lv W, Wei W, Li Z, Li B, Kang F, Yang Q-H (2013) A unique carbon with a high specific surface area produced by the carbonization of agar in the presence of graphene. *Chem Commun* 49(88):10427–10429
29. Cheng HKF, Sahoo NG, Tan YP, Pan Y, Bao H, Li L, Chan SH, Zhao J (2012) Poly (vinyl alcohol) nanocomposites filled with poly (vinyl alcohol)-grafted graphene oxide. *ACS Appl Mater Interfaces* 4(5):2387–2394
30. Kahr G, Madsen F (1995) Determination of the cation exchange capacity and the surface area of bentonite, illite and kaolinite by methylene blue adsorption. *Appl Clay Sci* 9(5):327–336
31. Cherifi Z, Boukoussa B, Zaoui A, Belbachir M, Meghabar R (2018) Structural, morphological and thermal properties of nanocomposites poly (GMA)/clay prepared by ultrasound and in-situ polymerization. *Ultrason Sonochem* 48:188–198
32. Vijayaraghavan K, Padmesh T, Palanivelu K, Velan M (2006) Biosorption of nickel (II) ions onto *Sargassum wightii*: application of two-parameter and three-parameter isotherm models. *J Hazard Mater* 133(1–3):304–308
33. Ouasfi N, Zbair M, Bouzikri S, Anfar Z, Bensitel M, Ahsaine HA, Sabbar E, Khamliche L (2019) Selected pharmaceuticals removal using algae derived porous carbon: experimental, modeling and DFT theoretical insights. *RSC Adv* 9(17):9792–9808
34. Song H, Chang Y, Wan X, Dai M, Song H, Jin Z (2014) Equilibrium, kinetic, and thermodynamic studies on adsorptive desulfurization onto CuCeIVY zeolite. *Ind Eng Chem Res* 53(14):5701–5708
35. Gunay A (2007) Application of nonlinear regression analysis for ammonium exchange by natural (Bigadiç) clinoptilolite. *J Hazard Mater* 148(3):708–713
36. Choy KK, Porter JF, McKay G (2004) Single and multicomponent equilibrium studies for the adsorption of acidic dyes on carbon from effluents. *Langmuir* 20(22):9646–9656
37. Foo KY, Hameed BH (2010) Insights into the modeling of adsorption isotherm systems. *Chem Eng J* 156(1):2–10
38. Tan K, Hameed B (2017) Insight into the adsorption kinetics models for the removal of contaminants from aqueous solutions. *J Taiwan Inst Chem Eng* 74:25–48
39. Abdelkrim S, Mokhtar A, Djelad A, Bennabi F, Souana A, Bengueddach A, Sassi M (2019) Chitosan/Ag-bentonite nanocomposites: preparation, characterization, swelling and biological properties. *J Inorg Organomet Polym Mater* 30:831–840
40. Abas SNA, Ismail MHS, Siajam SI, Kamal ML (2015) Comparative study on adsorption of Pb (II) ions by alginate beads and mangrove-alginate composite beads. *Ad Mater Res*. <https://doi.org/10.4028/www.scientific.net/AMR.1113.248>
41. Lyons JG, Geever LM, Nugent MJ, Kennedy JE, Higginbotham CL (2009) Development and characterisation of an

- agar–polyvinyl alcohol blend hydrogel. *J Mech Behav Biomed Mater* 2(5):485–493
42. Paluszkiwicz C, Holtzer M, Bobrowski A (2008) FTIR analysis of bentonite in moulding sands. *J Mol Struct* 880(1–3):109–114
  43. Alabarse FG, Conceição RV, Balzaretta NM, Schenato F, Xavier AM (2011) In-situ FTIR analyses of bentonite under high-pressure. *Appl Clay Sci* 51(1–2):202–208
  44. Moussout H, Ahlafi H, Aazza M, Zegaoui O, El Akili C (2016) Adsorption studies of Cu (II) onto biopolymer chitosan and its nanocomposite 5% bentonite/chitosan. *Water Sci Technol* 73(9):2199–2210
  45. Pal K, Banthia AK, Majumdar DK (2007) Preparation and characterization of polyvinyl alcohol-gelatin hydrogel membranes for biomedical applications. *Aaps Pharmscitech* 8(1):E142–E146
  46. Rhim JW, Lee SB, Hong SI (2011) Preparation and characterization of agar/clay nanocomposite films: the effect of clay type. *J Food Sci* 76(3):N40–N48
  47. Bilal M, Asgher M, Shahid M, Bhatti HN (2016) Characteristic features and dye degrading capability of agar agar gel immobilized manganese peroxidase. *Int J Biol Macromol* 86:728–740
  48. Wang H, Li C, Peng Z, Zhang S (2011) Characterization and thermal behavior of kaolin. *J Therm Anal Calorim* 105(1):157–160
  49. Shankar S, Teng X, Rhim J-W (2014) Properties and characterization of agar/CuNP bionanocomposite films prepared with different copper salts and reducing agents. *Carbohydr Polym* 114:484–492
  50. Roy S, Rhim J-W (2019) Agar-based antioxidant composite films incorporated with melanin nanoparticles. *Food Hydrocoll* 94:391–398
  51. Diebold U (2003) The surface science of titanium dioxide. *Surf Sci Rep* 48(5–8):53–229
  52. Liao D, Wu G, Liao B (2009) Zeta potential of shape-controlled TiO<sub>2</sub> nanoparticles with surfactants. *Colloids Surf A* 348(1–3):270–275
  53. Ma D, Zhu B, Cao B, Wang J, Zhang J (2017) Fabrication of the novel hydrogel based on waste corn stalk for removal of methylene blue dye from aqueous solution. *Appl Surf Sci* 422:944–952
  54. Paulino AT, Guilherme MR, Reis AV, Campese GM, Muniz EC, Nozaki J (2006) Removal of methylene blue dye from an aqueous media using superabsorbent hydrogel supported on modified polysaccharide. *J Colloid Interface Sci* 301(1):55–62
  55. Li W, Ma Q, Bai Y, Xu D, Wu M, Ma H (2018) Facile fabrication of gelatin/bentonite composite beads for tunable removal of anionic and cationic dyes. *Chem Eng Res Des* 134:336–346
  56. Abid Z, Hakiki A, Boukoussa B, Launay F, Hamaizi H, Bengueddach A, Hamacha R (2019) Preparation of highly hydrophilic PVA/SBA-15 composite materials and their adsorption behavior toward cationic dye: effect of PVA content. *J Mater Sci* 54(10):7679–7691
  57. Tu NTT, Thien TV, Du PD, Chau VTT, Mau TX, Khieu DQ (2018) Adsorptive removal of Congo red from aqueous solution using zeolitic imidazolate framework-67. *J Environ Chem Eng* 6(2):2269–2280
  58. Oussalah A, Boukerroui A, Aichour A, Djellouli B (2019) Cationic and anionic dyes removal by low-cost hybrid alginate/natural bentonite composite beads: adsorption and reusability studies. *Int J Biol Macromol* 124:854–862
  59. Wang L, Wang A (2007) Adsorption characteristics of Congo Red onto the chitosan/montmorillonite nanocomposite. *J Hazard Mater* 147(3):979–985
  60. Cheng B, Le Y, Cai W, Yu J (2011) Synthesis of hierarchical Ni(OH)<sub>2</sub> and NiO nanosheets and their adsorption kinetics and isotherms to Congo red in water. *J Hazard Mater* 185(2–3):889–897
  61. Samiey B, Ashoori F (2012) Adsorptive removal of methylene blue by agar: effects of NaCl and ethanol. *Chem Cent J* 6(1):14
  62. Yokwana K, Kuvarega AT, Mhlanga SD, Nxumalo EN (2018) Mechanistic aspects for the removal of congo red dye from aqueous media through adsorption over n-doped graphene oxide nanoadsorbents prepared from graphite flakes and powders. *Phys Chem Earth A/B/C* 107:58–70
  63. Fu J, Xin Q, Wu X, Chen Z, Yan Y, Liu S, Wang M, Xu Q (2016) Selective adsorption and separation of organic dyes from aqueous solution on polydopamine microspheres. *J Colloid Interface Sci* 461:292–304
  64. Kumar R, Ansari SA, Barakat M, Aljaafari A, Cho MH (2018) A polyaniline@ MoS<sub>2</sub>-based organic–inorganic nanohybrid for the removal of Congo red: adsorption kinetic, thermodynamic and isotherm studies. *New J Chem* 42(23):18802–18809

**Publisher's Note** Springer Nature remains neutral with regard to jurisdictional claims in published maps and institutional affiliations.